Synthesis and investigation of TiO2/g-C3N4 performance for photocatalytic degradation of Bromophenol Blue and Eriochrome Black T: Experimental design optimization and reactive oxygen species contribution

Fadimatou Hassan, Pierre Bonnet, Jean Marie Dangwang Dikdim, Nadège Gatcha-Bandjoun, Christophe Caperaa, Sadou Dalhatou, Abdoulaye Kane, Hicham Zeghioud

water

MDPI

Article

Synthesis and Investigation of TiO_2/g-C_3N_4 Performance for Photocatalytic Degradation of Bromophenol Blue and Eriochrome Black T: Experimental Design Optimization and Reactive Oxygen Species Contribution

Fadimatou Hassan [1,2], Pierre Bonnet [3], Jean Marie Dangwang Dikdim [2], Nadege Gatcha Bandjoun [2], Christophe Caperaa [3], Sadou Dalhatou [2], Abdoulaye Kane [1,*] and Hicham Zeghioud [1,*]

[1] UniLaSalle-Ecole des Métiers de l'Environnement, Cyclann, Campus de Ker Lann, 35170 Bruz, France
[2] Department of Chemistry, Faculty of Science, University of Maroua, Maroua 814, Cameroon
[3] Institut de Chimie de Clermont-Ferrand (ICCF), Université Clermont Auvergne, 24 Avenue Blaise Pascal, 63178 Aubiere, France
* Correspondence: abdoulaye.kane@unilasalle.fr (A.K.); hicham.zeghioud@unilasalle.fr (H.Z.)

Abstract: Graphitic carbon nitride (g-C_3N_4) based photocatalyst was synthesized and the photocatalytic performance was investigated for the removal of Eriochrome Black T (EBT) and Bromophenol Blue (BPB) under UV irradiation. The prepared materials were characterized by SEM-EDX, XRD, Raman, FTIR and DRS. Higher degradation efficiency for the same initial concentrations of EBT and BPB in presence of TiO_2/g-C_3N_4 have been achieved within 160 min of irradiation. The kinetic study showed that the photodegradation of BPB by TiO_2/g-C_3N_4 follows pseudo-first-order kinetics with an R2 value of 0.98. The addition of persulfate (PS) in BPB solution improved the degradation yield from 8.81% to 80.14% within 20 min of UV light irradiation. A Box-Behnken model was developed from three factors and Response surface methodology (RSM) was employed to identify the optimum conditions for the treatment of BPB solution by TiO_2/g-C_3N_4. The experimental values of degradation of BPB agreed with predicted values obtained from central composite design (CCD) analysis with an R^2 value of 0.9999. The scavenger study revealed that superoxide radical anion ($O_2^{\bullet -}$) plays a key role (68.89% of contribution) followed by $OH^{\bullet}$ and h^+ with 22.40% and 15.55% of contribution, respectively. This study has obviously exhibited the potential of TiO_2/g-C_3N_4 composite as a promising catalyst for photocatalytic purposes.

Keywords: photocatalysis; TiO_2/g-C_3N_4; bromophenol blue; Eriochrome Black T; dye degradation

Citation: Hassan, F.; Bonnet, P.; Dangwang Dikdim, J.M.; Gatcha Bandjoun, N.; Caperaa, C.; Dalhatou, S.; Kane, A.; Zeghioud, H. Synthesis and Investigation of TiO_2/g-C_3N_4 Performance for Photocatalytic Degradation of Bromophenol Blue and Eriochrome Black T: Experimental Design Optimization and Reactive Oxygen Species Contribution. *Water* **2022**, *14*, 3331. https://doi.org/10.3390/w14203331

Academic Editor: Chengyun Zhou

Received: 20 September 2022
Accepted: 18 October 2022
Published: 21 October 2022

1. Introduction

Water is a natural resource essential to human life. However, the scarcity of this precious resource has become a major problem faced by most countries in the world. This is usually due to the contamination of its sources by wastewater from human activities, mainly industry and agriculture [1]. Several pollutants found in water are organic in nature, such as dyes which are used in the textile and printing industries [2]. About 15–20% of dyes are lost during the dyeing process and therefore end up in the environment and can become a source of pollution [3]. Pharmaceutical pollutants such as drugs are also found in water when they are unmetabolized, and can be considered pollutants if their by-products are discharged into the environment [4].

The presence of pollutants in the water can be very toxic for living beings, causing health problems such as cancerogenic diseases, hepatitis, cholera and other diarrheal disease [5]. Therefore, the removal of these toxic organic pollutants from water is essential to protect public health. Reverse osmosis, ion exchange, electro-dialysis, electrolysis, coagulation, flocculation and adsorption are examples of some conventional methods commonly used for the removal of pollutants from water [6,7]. Adsorption is an effective

technology for the removal of organic and pharmaceutical pollutants from water [8–11]. In adsorption, pollutants from water adhere to the surface of an adsorbent to purify the water, the pollutants are not eliminated but transferred to the surface the adsorbent which may be considered as another possible future source of pollution [12].

Advanced Oxidation Processes (AOPs) are also promising methods for removal of contaminants from wastewater effluents due to their fast reaction rate and strong oxidation capability [13]. There exists a variety of AOPs, such as Fenton [14], ozonation or catalytic ozonation [15], photocatalysis [16], electrochemical oxidation [17], discharge plasma [18], Sonolysis [19] and ionizing radiation [20]. Among AOPs, photocatalysis is widely studied for wastewater treatment. Thus, our interest in this present work to focus on the photocatalysis which has is an emerging technology for the degradation of organic pollutants in wastewater [21,22].

Part of photocatalysis is the use of catalysts to enhance removal of organic pollutants in wastewater. Due to the increase in demand for catalysts with high performance in photocatalytic degradation of organic compounds, researchers have been looking for means to synthesize new catalysts or modify the existing ones to increase their photocatalytic activities [23]. Various oxidants were used in order to intensify the degradation performance of photocatalyst as reported in different works such as such as H_2O_2, O_2 and $K_2S_2O_8$ [24,25]. Photocatalytic activated persulfates system was reported to have the merits of environmental protection, a great chemical stability and a sustainability [26]. For example, Sun et al. reported an increase of 75% in quinoline degradation efficiency with increasing persulfate concentration in WO_3-$CuFe_2O_4$ Z-scheme system within 150 min [27].

Over these years, researchers have developed an interest in graphitic carbon nitride (g-C_3N_4) catalyst in the photocatalytic treatment of pollutants in water [28]. g-C_3N_4 is a low-cost metal-free polymer with properties such as facile synthesis, high stability, unique optical and electronic characteristics which makes g-C_3N_4-based catalysts suitable candidates for photocatalytic applications [29]. Semiconducting metal oxides such as TiO_2 are known to be efficient in the degradation of organic pollutants and combining it with other compounds may increase their photocatalytic activities [30,31]. To promote the photocatalytic performance of TiO_2, different strategies were used, such as surface modification, doping, morphology control, facet engineering, coupling different semiconductors and adding oxidants (i.e., H_2O_2, O_3, and persulfate) [32,33]. Herein, the last two strategies were adopted to achieve these objectives. Indeed, coupling g-C_3N_4 with TiO_2 can increase the reaction site on the surface of g-C_3N_4, and can also act as an active site to promote the transfer of radical species [34,35]. Heterojunction composites like TiO_2/g-C_3N_4 help to reduce electron-hole recombination rate which leads to increase in photocatalytic reactions [36]. Such catalysts have been widely used in the photocatalytic hydrogen production [37], to enhance visible photocatalytic activity [38] and in the degradation of organic pollutants [39]. Eriochrome Black T (EBT) and Bromophenol Blue (BPB) used in printings, pharmaceutical and textiles industries as dyes, They are commonly used to evaluate the photocatalytic performance of semiconductor materials in aqueous media [16,40–42].

In this study, a simple synthesis route of g-C_3N_4 based catalysts (g-C_3N_4, 30% TiO_2/g-C_3N_4) were tested and the degradation performances of obtained photocatalysts were studied on the removal of EBT and BPB solutions. The behavior of TiO_2/g-C_3N_4 toward BPB degradation under in influence of a simultaneous different variable parameters was examined via Response Surface methodology (RSM). Furthermore, the potential of TiO_2/g-C_3N_4 in the degradation of dye solutions under various conditions (catalyst dosage, dye concentration, pH values, presence of salt and some oxidants) were also studied. Kinetics of photocatalytic degradation was studied and the contribution of active species in the degradation process was investigated.

2. Materials and Methods

2.1. Materials

Chemicals used for this study were: Bromophenol blue was purchased from REACTIF RAL (Paris, France), Eriochrome Black T and sodium persulfate ($Na_2S_4O_8 \geq 98.0\%$) were obtained from PROLABO (Paris, French), Hydrogen peroxide (H_2O_2, 30%, from Millipore, Darmstadt, Germany), sodium chloride ($NaCl \geq 99.0\%$, purchased from SIGMA-ALDRICH, Missouri, USA), hydrochloric acid ($HCl \geq 37\%$, from Honeywell, Seelze, Germany), sodium hydroxide (NaOH, 98% purity) were purchased from Sigma–Aldrich (Grenoble, French). Isopropanol ($C_3H_8O \geq 99.7\%$) and methanol ($CH_4O \geq 99.8\%$) obtained from MERCK company (Darmstadt, Germany) and potassium dichromate ($K_2Cr_2O_7 \geq 99.5\%$) purchased from Panreac (Barcelone, Spain). All the solutions were prepared using reverse osmosis water. Eriochrome black t and Bromophenol blue properties are shown in the Table 1:

Table 1. Physico-chemical properties of Eriochrome black t and Bromophenol blue.

Dye	Molecular Formula	Structure	λ Max
Eriochrome black t	$C_{20}H_{12}N_3O_7SNa$	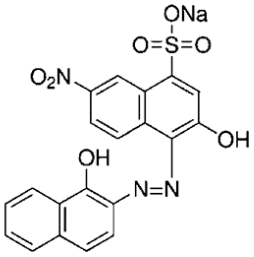	535 nm
Bromophenol blue	$C_{19}H_{10}Br_4O_5S$	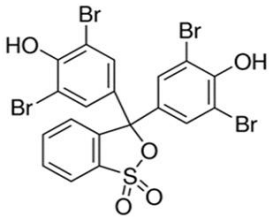	592 nm

2.2. Synthesis of g-C_3N_4 and TiO_2/g-C_3N_4 Composites

The synthesis of bulk g-C_3N_4 was done by thermal polymerization based on the previous work [43,44]. Briefly, g-C_3N_4 was synthesized by thermal polymerization where 10 g of dicyandiamide was placed into an alumina crucible, and then heated at 550 °C in a muffle furnace during 4 h (20 °C/min). Afterward cooled to room temperature, the obtained solid was grinded into powders for further usage.

The synthesis of TiO_2 was done by the sol-gel method inspired by the work of Askari et al. [45]. Briefly, titanium isopropoxide was dissolved in acetic acid and the mixture was maintained under stirring. The reverse osmosis water was added drop by drop for the hydrolysis. The resultant gel was dried at 200 °C for 2 h. The TiO_2 nanoparticles were obtained after calcination of the sample at 400 °C during 4 h in order to improve the crystallinity of the nanoparticles.

However the TiO_2/g-C_3N_4 composite was prepared by wet- impregnation according to the literature [46,47]. In which, a suitable quantity of g-C_3N_4 and TiO_2 were dissolved separately in methanol and then, sonificated in an ultrasonic bath during 30 min. The two solutions were mixed and stirred at room temperature for 24 h. The resultant powder was preserved under room temperature for 12 h eliminate solvent by evaporation.

The schematic illustration of the materials preparation was regrouped in Figure 1.

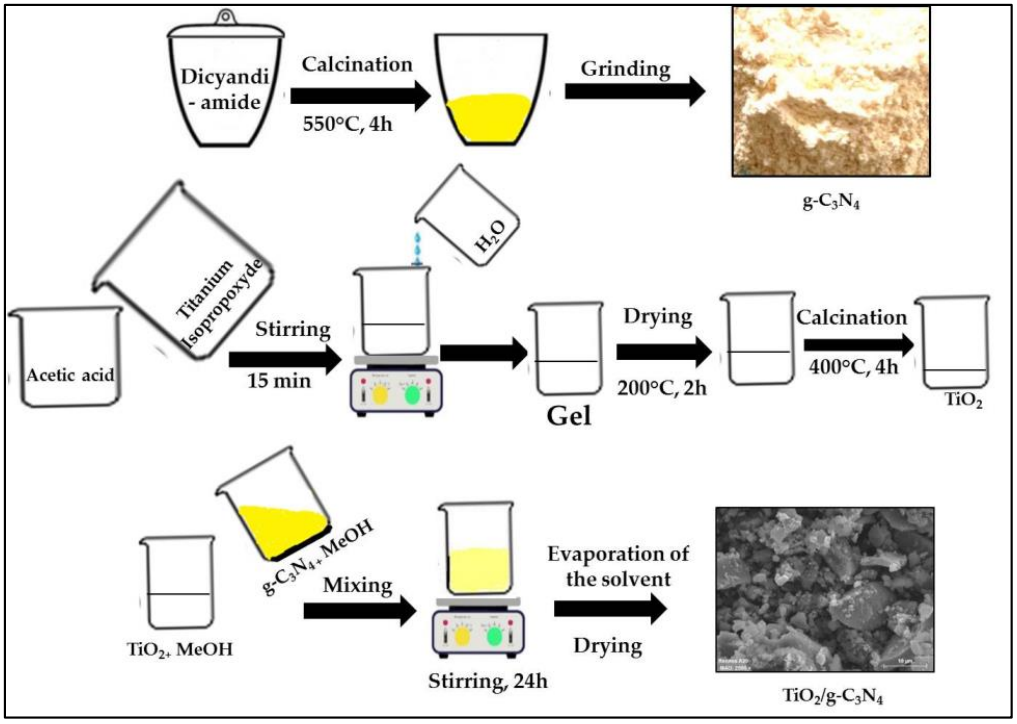

Figure 1. Schematic illustration of the preparation of materials.

2.3. Photocatalytic Treatment

EBT and BBP solutions used in the experiments were prepared at different concentrations (2, 5, 10 and 12 ppm). Photodegradation experiments were performed in the batch system of 1000 mL beaker and stirred at 400 rpm. The mass of the catalyst was dispersed into a volume of 500 mL solutions. The mixture was left in the dark and continuously stirred for 30 min to achieve the adsorption-desorption equilibrium before UV irradiation (UVA lamp of 24 W with wavelength of 365 nm as reported in Figure S1). After reaching the adsorption-desorption equilibrium, the dye solution was then exposed to UV-light for 180 min. At 20 min time intervals, 3 mL samples of the solution were collected from the photoreactor and filtered to remove the photocatalysts by a syringe filter (pore size 0.45 µm).

A dual-beam spectrophotometer (SHIMADZU UV-1800) was used to measure the absorbance at maximum wavelengths of 535 nm and 592 nm for EBT and BPB, respectively (example of BPB degradation in Figure S2). The photodegradation rate was estimated using the following equation:

$$R\ (\%) = \frac{C_0 - C_t}{C_0} \times 100 \quad (1)$$

where C_0 is the initial concentration of pollutant in mg/L and C_t is the concentration of dyes in mg/L at time t. For all photocatalytic experiments the pH value was adjusted only at the beginning of the experiment. The pH of the solution was adjusted by HCl and NaOH (0.01 M).

All figures (at the exception of figures generated from RSM study) was drawn using OriginPro 2022, from OriginLab Corporation, Northampton, MA, USA.

2.4. Photocatalyst Characterization

- The X-ray diffraction (XRD) patterns of as-prepared catalysts were made using a D8 Bruker spectrometer (Cu Ka radiation with wavelength λ = 0.15418 nm as a wavelength) the incident angle of 2θ, 5–130° using 0.017° each step, and the acceleration tension is 40 kV and current emission equals 30 mA.

- Raman spectra were acquired by using Raman spectrometer of JobinYvon company model T64000. The wavelength of laser was 514.5 nm (2.41 eV) and the power was set at 100 mW. The measurement was carried out in solid state by dispersing the sample powder upon glass slide under air at room temperature.
- The scanning electron microscopy (SEM) images of the photocatalysts were obtained using an (JEOL 5910 LV) apparatus with EDS elementary analysis using SDD detector (Bruker)
- The UV–vis diffuse reflectance spectra (UV–vis DRS) of the photocatalysts were recorded by Cary 300 instrument with scan Rate of 600 nm/min in shifting range of 80 to 500 cm^{-1}.

3. Results and Discussion

3.1. Characterization of Photocatalyst

The SEM images and EDX spectrum of the photocatalytic materials were shown in Figure 2. It seems that g-C_3N_4 and TiO_2/g-C_3N_4 were composed of many stacked particles, which presented an irregular spherical shapes morphology with more homogeneity for g-C_3N_4. Moreover, g-C_3N_4 particles appear as platelets, which is in good agreement with the 2D structure however in TiO_2/g-C_3N_4 images in addition to the observed platelets there are small particles which may be attributed to TiO2. Images presented also a porous surface with various sizes. EDX spectrum confirmed the presences of C, N and O elements in g-C3N4 sample, and the presence of C, N, O and Ti for TiO_2/g-C_3N_4 composite sample. This may demonstrate that both photocatalyst composites were well synthesized.

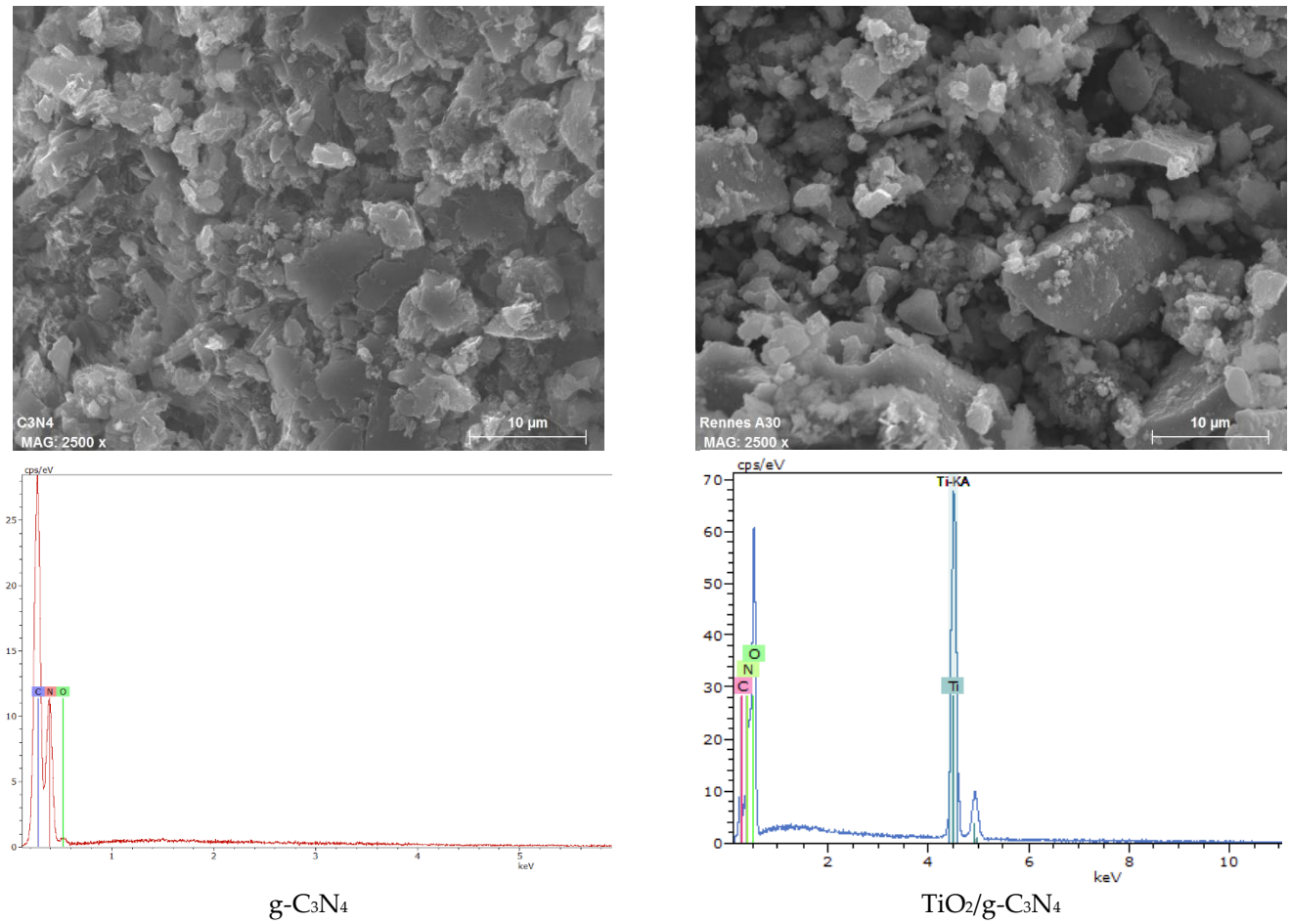

g-C_3N_4 TiO_2/g-C_3N_4

Figure 2. SEM images with EDX spectra of g-C3N4 and TiO_2/g-C_3N_4.

The crystallinity structure of the synthesized materials g-C_3N_4 and g-C_3N_4 modified TiO_2 nanocomposites were characterized and the results were shown in Figure 3a. The XRD pattern of TiO_2/g-C_3N_4 revealed numerous peaks at 25.3°, 37.8°, 48.1°, 54.0°, 55.1°, 62.8°, 68.9°, 70.1°, 75.3° and 83.2°, corresponding to the diffraction planes of (101), (004), (200), (105), (211), (204), (116), (220) and (215) which corresponds to the anatase phase JCPDS 21-1272 [44,48]. The g-C_3N_4 shows the diffraction peaks at 12.8° and 27.57°, corresponds to the inter-plane structural packing motif (100) and the interlayer diffraction plane (002) of the hexagonal graphitic carbon nitride [49]. However, while adding the g-C_3N_4 to the TiO_2 the intensity of g-C_3N_4 peaks was relatively narrowed compared to TiO_2 peaks in the composite. The result confirmed that the crystallinity structure of TiO_2 is highly reduced in TiO_2/g-C_3N_4 composites [50].

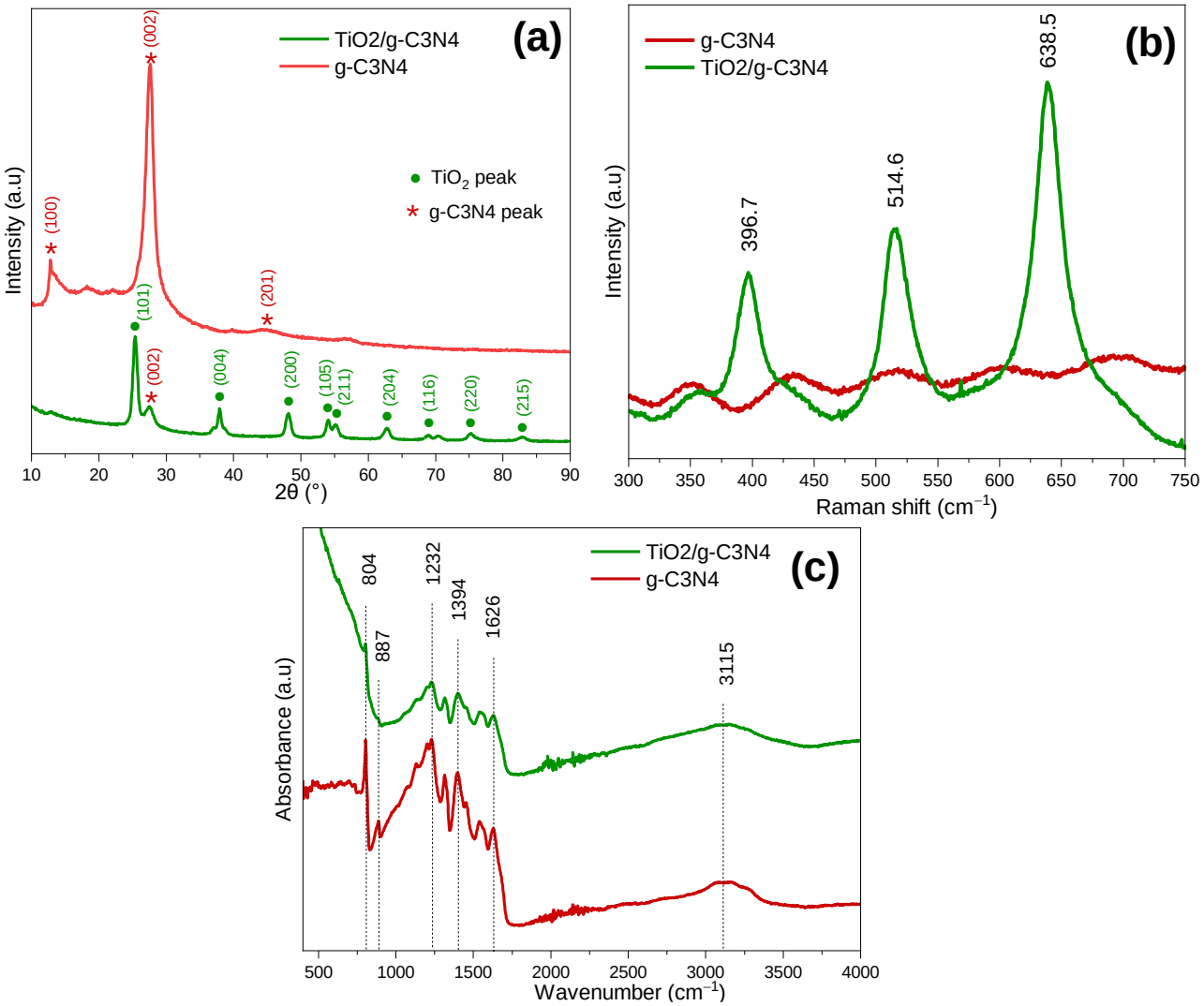

Figure 3. (**a**) XRD patterns of materials; (**b**) Raman spectra and (**c**) FTIR spectra of g-C_3N_4 and TiO_2/g-C_3N_4 composites.

Raman spectra of photocatalytic materials are shown in Figure 3b. Theses spectra were recorded to obtain more structural information on synthesized composite. Three characteristic Raman active modes of anatase crystalline form of TiO2 with symmetries B1g, A1g and Eg were detected at 396.7, 514.6 and 638.5 cm^{-1}, respectively [51]. The presence of these characteristic vibrational frequencies and their relative intensity confirmed the phase pure anatase TiO_2. These results are in an agreement with XRD analyses and confirm

the formation of phase pure anatase TiO_2 [52]. The spectrum of g-C_3N_4 did not present exploitable peaks in this zone.

FTIR spectra of g-C_3N_4 and TiO_2/g-C_3N_4 composites with different g-C_3N_4 contents are presented in Figure 3c. Pure g-C_3N_4 shows characteristic IR peaks similar to those of the previous results [53,54]. The peak at 1640 cm^{-1} is assigned to C=N stretching vibration mode, while those at 1247, 1325 and 1408 cm^{-1} are associated with C−N heterocycle stretching of g-C_3N_4, fully condensed C–N moieties/partially condensed C–NH moieties and aromatic C−N heterocycles, respectively [55]. The peak at 808 cm^{-1} can be attributed to the characteristic bending mode of s-triazine ring system [54]. A broad band in the range of 3150–3300 cm^{-1} corresponds to the stretching vibration modes of terminal $-NH_2$ and −NH− groups [56]. Pure TiO_2 shows characteristic broad absorption band at 500–700 cm^{-1} [57]. It can be clearly seen that the main characteristic peaks of g-C_3N_4 and TiO_2 appeared in TiO_2/g-C_3N_4 sample suggesting the formation of a composite between g-C_3N_4 and TiO_2 [58].

The UV–Vis DRS spectra of g-C_3N_4 and TiO_2/g-C_3N_4 were presented in Figure 4. It can be seen that a combination of TiO_2 and g-C_3N_4 could significantly change the absorption band of composites compared to that of g-C_3N_4 or TiO_2 components. Accordingly, the presence of g-C_3N_4 in the composite gives to TiO_2 the capacity for absorbing light in visible region rather than UV region. Based on these data, the band gap values for g-C_3N_4 and TiO_2/g-C_3N_4 were calculated as 2.65 eV and 2.48 eV, respectively.

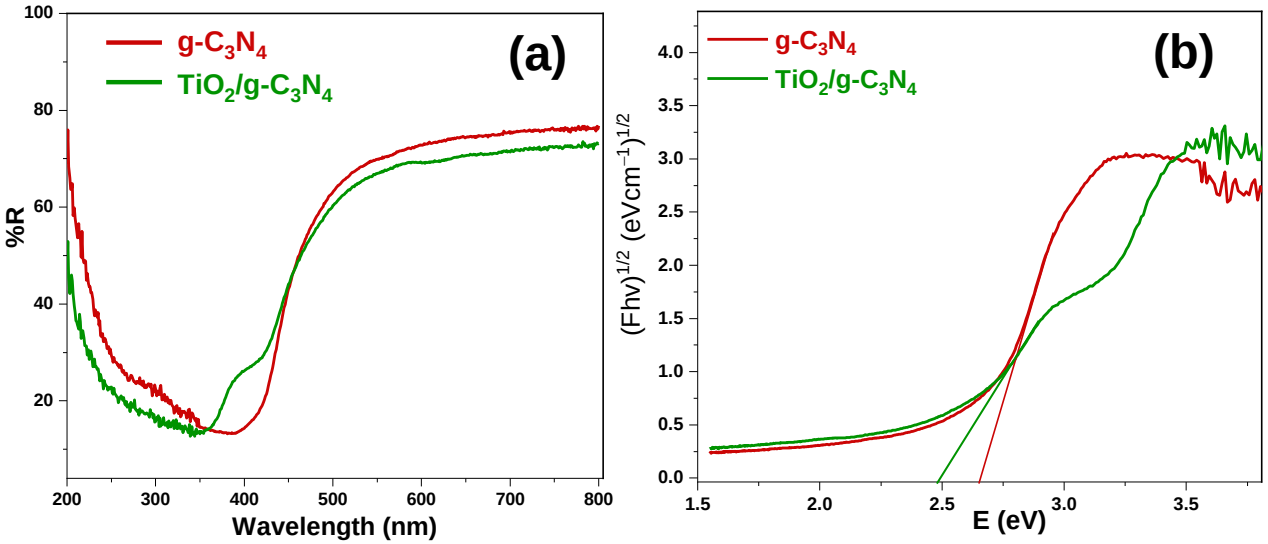

Figure 4. Diffuse Reflectance Spectra (**a**) and plot of transferred Kubelka-Munk versus energy of the light absorbed (**b**) of pure g-C_3N_4 and TiO_2/g-C_3N_4.

3.2. Catalyst Activity

The photocatalytic performances of the catalysts were evaluated by the photodegradation of 10 ppm solutions of EBT and BPB as pollutants using UV light and 200 mg/L of catalyst. For EBT, under UV light irradiation, we obtained a higher degradation efficiency after 180 min with TiO_2/g-C_3N_4 followed by g-C_3N_4, for both dyes. From Figure 5, we observed that degradation efficiencies of EBT are 87.94% and 100% for g-C_3N_4 and TiO_2/g-C_3N_4, respectively.

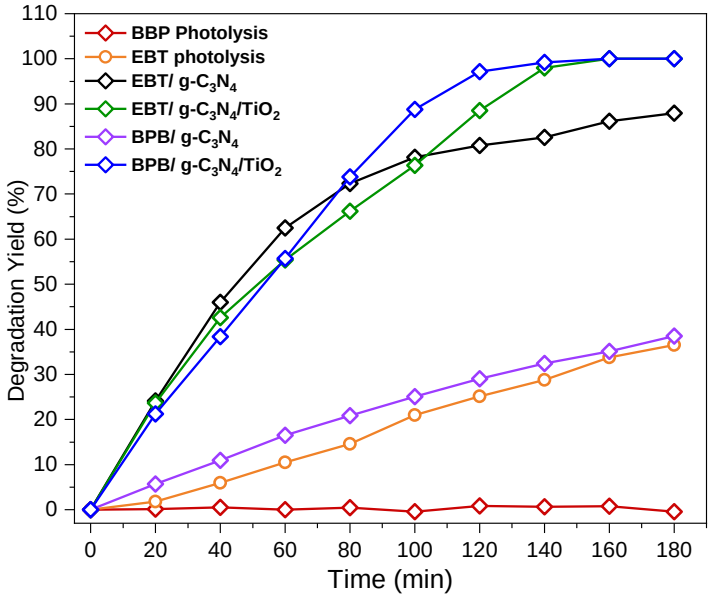

Figure 5. Photodegradation of 500 mL of dye solution (10 ppm) with 200 mg/L of catalyst under UV irradiation and natural pH.

For BPB, we observe a degradation efficiency of 38.53% and 100% for g-C_3N_4 and TiO_2/g-C_3N_4, respectively. There is a significant difference in the degradation efficiency of the dyes when using g-C_3N_4 with 87.94% and 38.53% for EBT and BPB, respectively. These results may be attributed to the fact that under UV light irradiation and in the absence of catalyst, we observe 36% degradation of EBT, while no degradation of BPB. From another hand, EBT and BPB belong to the Azo and sulphonephthalein families respectively and therefore differ in their physico-chemical properties. It is easier to break the unsaturated bonds of BPB than those of EBT (azo bonds).

A comparative table of photocatalytic degradation of dyes with g-C_3N_4 based photocatalyst with different light sources is shown in Table 2 below:

Table 2. Comparison of photocatalytic activity of g-C_3N_4 based photocatalysts.

Photocatalyst	Pollutant	Degradation Efficiency (%)	Light Source	Reference
40 wt% g-C_3N_4/Ag_3VO	Basic Fuchsin	95.0	Visible	[59]
g-C_3N_4/TiO_2(NT)	Rhodamine B	96.7	Visible	[60]
g-C_3N_4-TiO_2	Rhodamine B	99.0	Visible	[61]
9 wt% Bi_2O_3/porous g-C_3N_4	Reactive Black 5	84.0	UV-vis	[62]
NP-GQDs-90/g-C_3N_4	Methyl Orange	96.0	UV	[63]
g-C_3N_4/TiO_2-1.5	Methylene Blue	95.3	UV	[64]
Nanosheet g-C_3N_4/CNMBGt	Methylene Blue	98.2	UV	[65]
g-C_3N_4	EBT	87.9	UV	Present work
TiO_2/g-C_3N_4	EBT	100.0	UV	Present work
g-C_3N_4	BPB	38.5	UV	Present work
TiO_2/g-C_3N_4	BPB	100.0	UV	Present work

3.3. Effect of Photocatalyst Dosage

In views of the results obtained during photolysis were BPB showed no sensitivity to UV-light compared to EBT, it was preferable to continue our studies for more precise

results with BPB. The effect of photocatalyst dosage was studied using 10 ppm of BPB solution. An increase in photocatalyst dosage from 50 mg/L to 200 mg/L increases BPB degradation efficiency from 58.17 to 100% during 180 min irradiation time as shown in Figure 6.The addition of catalyst results in an increase in the photocatalytic performance due to an increase in active sites which leads to an increase in radical species formation [66]. Excess dosage of catalyst into the reaction mixture may enhance light reflectance due to the increase of the solution turbidity, which in turn leads to preventing light absorption by the catalyst reducing the degradation rate [30,67,68]. The degradation efficiency increases rapidly with an increase in photocatalyst from 50 to 100 mg/L and increases slightly with an increase in photocatalyst from 100 to 200 mg/L after 180 min irradiation. In order to obtain high degradation efficiencies and avoid the use of excess catalyst, the quantity of photocatalyst chosen to continue our studies was 100 mg/L.

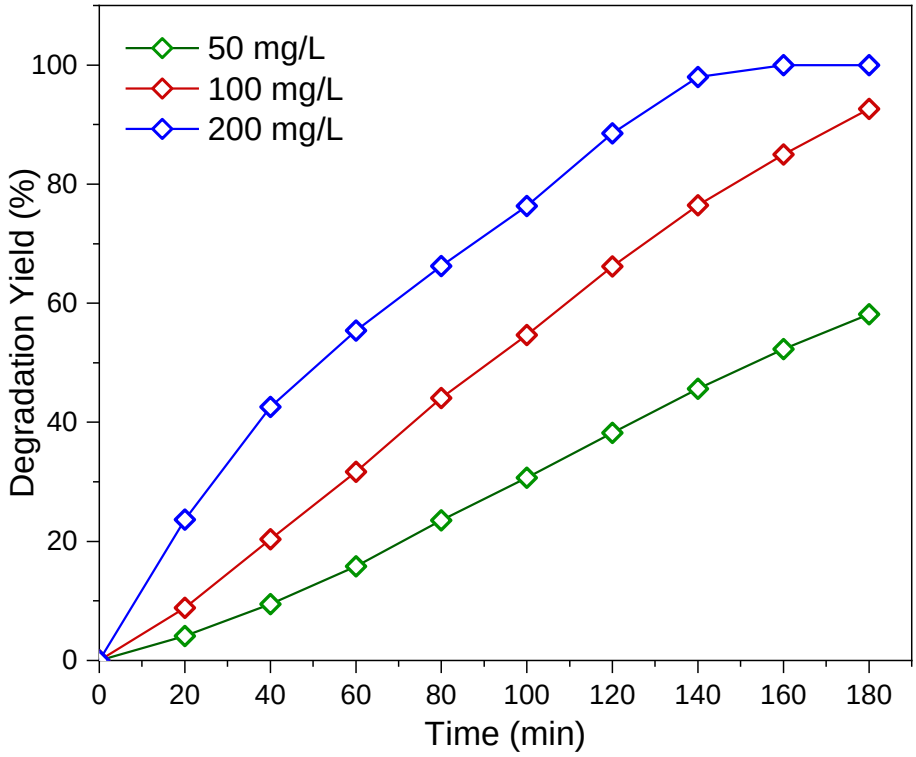

Figure 6. Effect of catalyst dosage in the photodegradation of BPB solution (10 ppm), natural pH, under UV irradiation.

3.4. Effect of Initial Dye Concentration

The effect of initial BPB concentration on degradation was explored under concentrations from 2 to 20 ppm with 100 mg/L of catalyst. Figure 7 shows that an increase in dye concentration from 2 to 20 ppm decreases overall degradation, from 100% to 27.33%.

This can be attributed to the quantity of active sites available when using the same quantity of catalyst for different dye concentration [69]. With low initial concentration, TiO_2/g-C_3N_4 provides a sufficient number of active sites for BPB molecules adsorption. With higher initial concentrations, the number of active sites provided by the TiO_2/g-C_3N_4 reduces, thus decreasing the degradation efficiency of the dye [70].

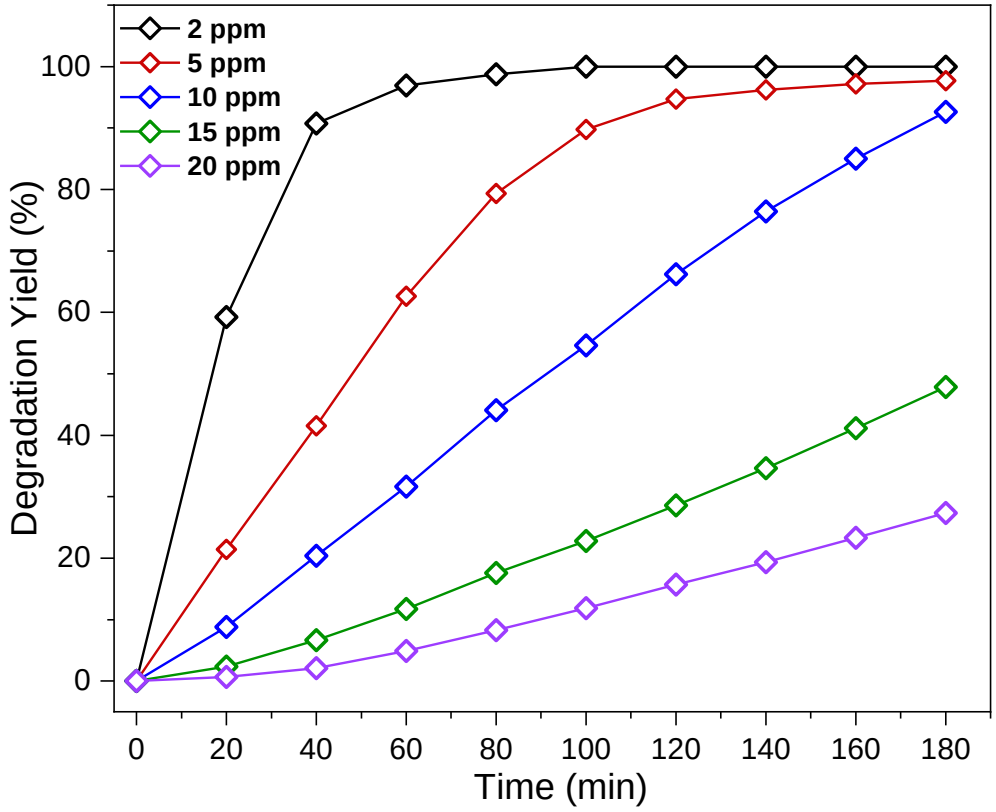

Figure 7. Effect of initial dye concentration with 500 mL of BPB solution, 100 mg/L of catalyst, natural pH, under UV irradiation.

The opacity of the solution at high concentration may also reduce the intensity of the light travelling through the system which leads to a decrease in the photocatalytic activity of the photocatalyst. Increasing dye concentration facilitates light adsorption by the dye molecules and reduces the amount of light reaching the surface of the catalyst, thus decreasing generation of active sites [71,72].

3.5. Kinetic Study

To determine BPB degradation kinetics, pseudo-first-order kinetic and Langmuir-Hinshelwood models were investigated. The kinetic parameters of the reaction were obtained using the pseudo-first-order kinetic model expressed as follows:

$$\ln(\frac{C_0}{C}) = k_1\, t \tag{2}$$

The terms k_1, C and C_0 are respectively the rate of pseudo-first-order reaction, expressed in min^{-1}, BPB concentration at the time t, expressed in mg/L, and BPB initial concentration, also in mg/L.

The pseudo-first-order (k_1) reaction rate was obtained from the linear plot of $\ln(C_0/C)$ versus time as seen in Figure 8. From Table 3, it can be seen that k_1 decreases with increase in initial concentration which is quite common in photocatalytic degradation of organic compounds in solution [73]. The correlation coefficients close to 1 ($R^2 > 0.95$) confirmed that photodegradation of BPB by TiO_2/g-C_3N_4 effectively follows a pseudo first-order kinetics model [74].

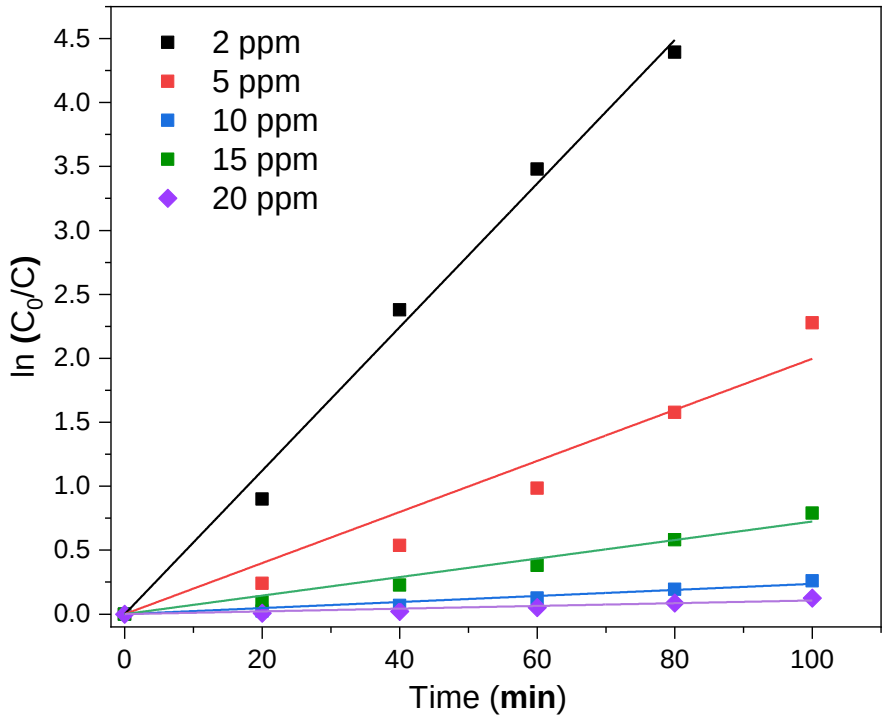

Figure 8. Pseudo-first-order kinetics for BPB at different initial concentration with 100 mg/L of catalyst under UV irradiation.

Table 3. Variation of the pseudo-first-order rate constant (k_1) at various initial concentration of BPB (C_0).

C_0 (mg/L)	k_1 (min^{-1})	R^2
2	0.0561	0.9976
5	0.0200	0.9756
10	0.0072	0.9881
15	0.0024	0.9837
20	0.0011	0.9516

Most heterogeneous photocatalytic degradation reactions follow Langmuir–Hinshelwood (L-H) kinetics to describe the relationship between initial degradation rate and initial concentration [75,76].The L-H model used in this study can be expressed as follow:

$$\frac{1}{r_0} = \frac{1}{k} + \frac{1}{kK}\frac{1}{C_0} \quad (3)$$

where k denotes the reaction rate constant for the process (mg L^{-1} min^{-1}), K is the adsorption coefficient of reactants (L mg^{-1}), C_0 is the initial concentration of dye (mg/L) and r_0 is the initial rate of disappearance of dye (mg L^{-1} min^{-1}).

A linear expression can be conveniently obtained by plotting the reciprocal initial rate against the reciprocal initial concentration. The slope is $1/(kK)$ and the intercept is $1/K$ (Figure 9). The linear transform of this expression yielded k = 0.108 mg L^{-1} min^{-1} and K = 0.0585 L mg^{-1}.

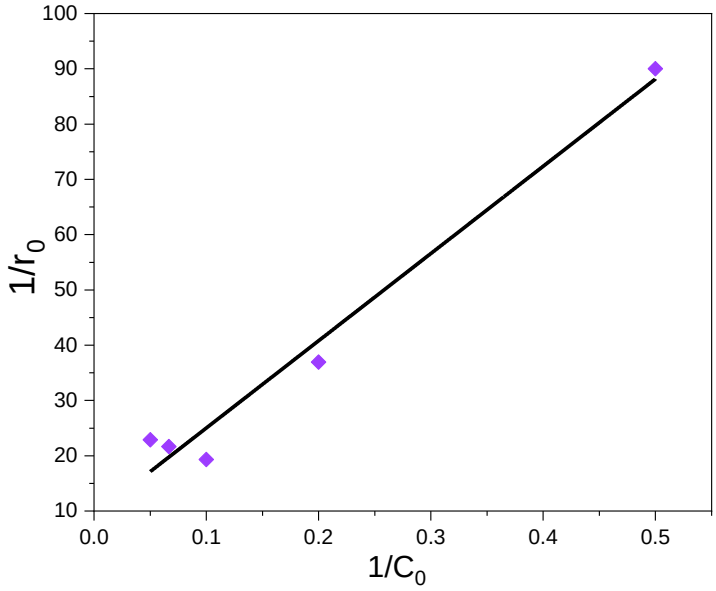

Figure 9. Linear correlation of $1/r_0$ versus $1/C_0$.

3.6. Effect of Persulfate

The effect of persulfate (PS) on the performance of TiO_2/g-C_3N_4 towards BPB degradation was evaluated by introducing 2.4 mmol/L of sodium persulfate ($Na_2S_2O_8$) in the suspension. In the first 20 min we observed a removal efficiency of 80.14% and 98.83% after 180 min irradiation (Figure 10). This improvement in removal efficiency comes from the presence of PS which inhibits the recombination of electron/hole pairs in the catalyst by capturing photo induced electrons [77]. Addition of PS accelerates the generation of radicals, thus boosting decontamination rate [67]. This can be explained by recent studies of persulfate activation of g-C_3N_4 and TiO_2 based catalysts.

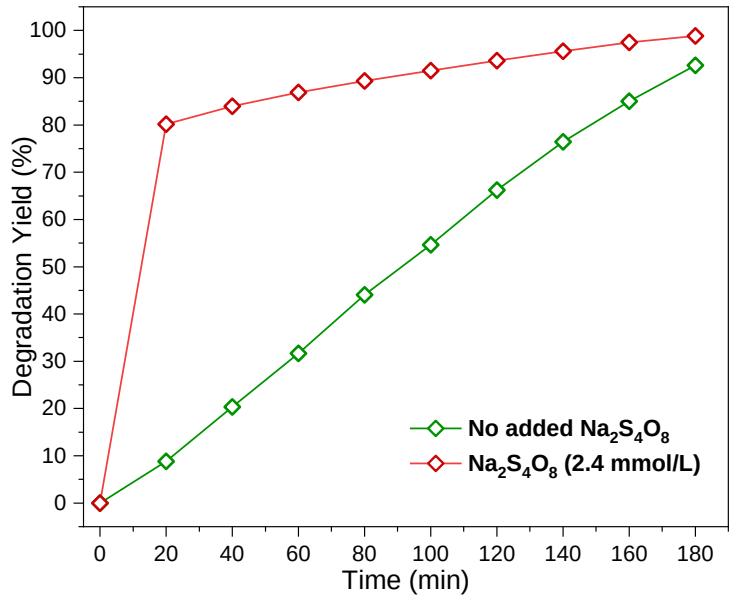

Figure 10. Effect of persulfate on the photodegradation of 500 mL BPB solution (10 ppm) with 100 mg/L of catalyst, natural pH, under UV irradiation.

A review on the activation of persulfate on g-C_3N_4-based catalyst for environmental remediation states that PS-captures photoinduced electrons of g-C_3N_4 and reduces electron-hole pairs recombination thereby increasing the formation of radicals which increases the

photodegradation of the pollutant (bisphenol A; BPA) [78]. This was further explained through the following reactions:

$$g\text{-}C_3N_4 + h\nu \rightarrow e^- + h^+ \quad (4)$$

$$e^- + O_2 \rightarrow O_2^{\bullet -} \quad (5)$$

$$e^- + S_2O_8^{-2} \rightarrow [\,S_2O_8^{-2}]^- \quad (6)$$

$$[S_2O_8^{-2}]^- + O_2 \rightarrow S_2O_8^{-2} + O_2^{\bullet -} \quad (7)$$

$$O_2^{\bullet -}/h^+ + \text{organic pollutants} \rightarrow \text{organic pollutants} \quad (8)$$

From the recent advances in persulfate-assisted TiO_2-based photocatalysis for wastewater treatment, TiO_2 can be excited to produce electron-hole pair and persulfate is then activated by photo-induced e^- to generate $SO_4^{\bullet -}$ radicals [33]. The h^+ can react with H_2O to produce hydroxyl radicals ($^\bullet$OH). Under UV light, persulfate can also be activated to form $SO_4^{\bullet -}$ radicals [79] which can also react with OH^- ions to form $^\bullet$OH radicals [80]. $SO_4^{\bullet -}$ and $^\bullet$OH radicals with strong oxidation ability can degrade organic pollutants in water, as explained in these reactions [33]:

$$TiO_2 + h\nu \rightarrow e^- + h^+ \quad (9)$$

$$h^+ + H_2O \rightarrow {}^\bullet OH + H^+ \quad (10)$$

$$S_2O_8^{2-} + h\nu \rightarrow 2SO_4^{\bullet -} \quad (11)$$

$$SO_4^{\bullet -} + OH^- \rightarrow SO_4^{2-} + {}^\bullet OH \quad (12)$$

$$SO_4^{\bullet -}/{}^\bullet OH + \text{organic pollutants} \rightarrow \text{degradation products} \quad (13)$$

3.7. Effect of pH, H_2O_2 and NaCl

Three-level CCD (low, central and high) with three factors was used for create a model for the photodegradation of BPB in the presence of $TiO_2/g\text{-}C_3N_4$ under UV-light. Barzegar et al., applied this design to express mathematical relationships among variables such as process time, catalyst mass and initial concentrations of methylene blue (MB) and rhodamine B (RhB) in the degradation process with $TiO_2/g\text{-}C_3N_4$ [35]. The model examined was made of 13 experiments to determine the contribution of the factors (A: pH, B: C_{H2O2}, C: C_{NaCl}) on photocatalytic degradation of BPB and Table 4 represents the obtained BPB removal percentage for each experimental run.

The experimental results obtained were represented also as a spider or radar graph visualization to better highlight the effect of different parameters on the degradation yield of BPB as shown in Figure 11. To get a good presentation the three studied parameters (pH, NaCl, and H_2O_2) was reported with theirs coded values (−1, 0 and 1) however the degradation yield was reported from zero to one. I t seems that a basic pH and hydrogen peroxide are suitable for a high BPB molecules degradation, nevertheless, the NaCl presence in some case have a negative effect and, in another case, have no effect in the dye elimination.

Table 4. Experimental design for the mutual effects of pH, NaCl, and H_2O_2 on photocatalytic degradation BPB by TiO_2/g-C_3N_4.

Run	Factor 1 A: pH	Factor 2 B: C_{H2O2} (mmol/L)	Factor 3 C: C_{NaCl} (mg/L)	Response Degradation %
1	7	0.4	5	28.69
2	11	0.4	10	18.44
3	7	2.4	5	14.26
4	11	2.4	10	67.52
5	3	0.4	10	80.60
6	7	2.4	15	6.06
7	3	1.4	15	77.59
8	11	1.4	15	65.87
9	7	1.4	10	10.00
10	7	0.4	15	21.56
11	3	2.4	10	80.70
12	3	1.4	5	80.88
13	11	1.4	5	57.54

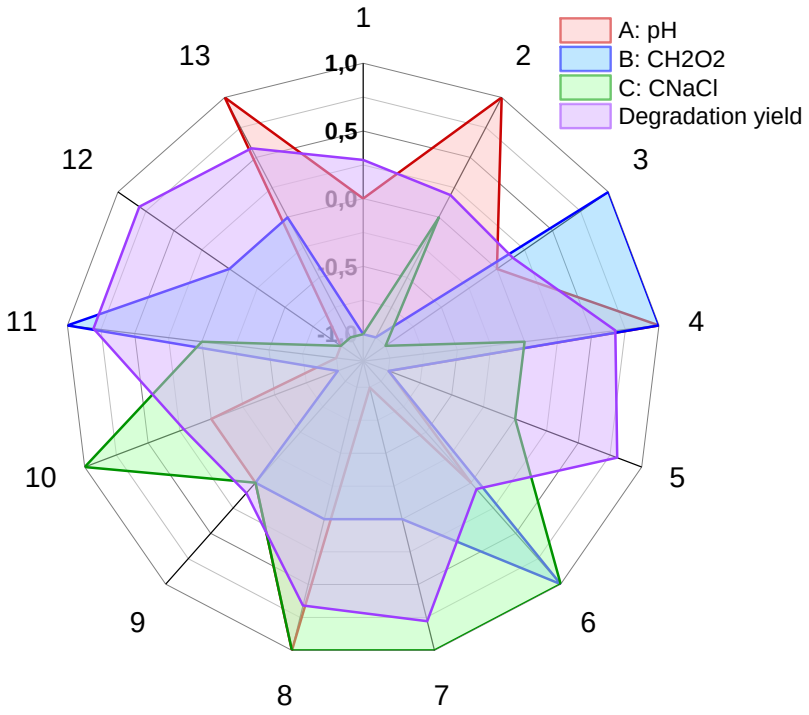

Figure 11. Spider graph visualization of experimental design results for the mutual effects of pH, NaCl, and H_2O_2 on photocatalytic degradation BPB by TiO_2/g-C_3N_4.

Response surface methodology (RMS) was applied to determine the best conditions for BPB degradation. A Box-Behnken design model was used to investigate the effects of 3 independent variables at three pH levels (3, 7, and 11), concentration of H_2O_2 (0.4, 1.4 and 2.4 mmol L^{-1}) and concentration of NaCl (5,10 and 15 mg L^{-1}). The modified quadratic model equation was as follows:

$$\%R \text{ degradation} = +108.56630$$

$$\begin{gathered} -13.20569 * pH + 31.65992 * C_{H2O2} + 8.74214 * C_{NaCl} \\ -14.24516 * pH * C_{H2O2} - 2.76016 * pH * C_{NaCl} \\ + 0.916335 * pH^2 - 0.370286 * C_{NaCl}{}^2 \\ 1.23617 * pH^2 * C_{H2O2} + 0.063672 * pH^2 * C_{NaCl} \\ + 0.100700 * pH * C_{NaCl}{}^2 \end{gathered} \quad (14)$$

The ANOVA results of BPB removal (%) by TiO_2/g-C_3N_4 composite is presented in the Table 5. As seen, the *p*-value of <0.0001 for the model signifies that the model is statistically significant and indicate that the applied mathematical model better fitted to the experimental data as confirmed by lack of fit [81]. To be determined as significant, *p*-value for a model parameter (individual or interaction) must be < 0.05. In this case, all the model terms are significant [81].

Table 5. ANOVA Table and goodness-of-fit coefficients for response variables.

Source	F-Value	*p*-Value
Model	2545.44	0.0004
A-pH	3239.21	0.0003
B-C_{H2O2}	511.38	0.0019
C-C_{NaCl}	134.20	0.0074
AB	1369.07	0.0007
AC	77.05	0.00127
A^2	17642.96	< 0.0001
C^2	447.28	0.0022
A^2B	1785.98	0.006
A^2C	118.45	0.0083
AC^2	462.95	0.0022

The Predicted R^2 of 0.9877 is in reasonable agreement with the Adjusted R^2 of 0.9995 (Table 6). Adequate Precision measures the signal to noise ratio. A ratio greater than 4 is desirable. The obtained ratio of 122,161 indicates an adequate signal, which confirm that this model can be used to navigate the design.

Table 6. Fit Statistics.

Parameter	Value
R^2	0.9999
Adjusted R^2	0.9995
Predicted R^2	0.9877
Adequate Precision	122.1613

A comparison of the experimental data to the predicted values by the refitted model was made through a predicted vs. actual plot, their closeness can be better observed in Figure 12. Data points were fragmented consistently on the diagonal line of 45° proving the goodness of fit. These results are similar to those obtained when using optimization approach in phosphoric acid-treated spent tea residue biochar for wastewater decoloring [82] and the sorption and removal of crude oil spills from seawater using peat-derived biochar [83].

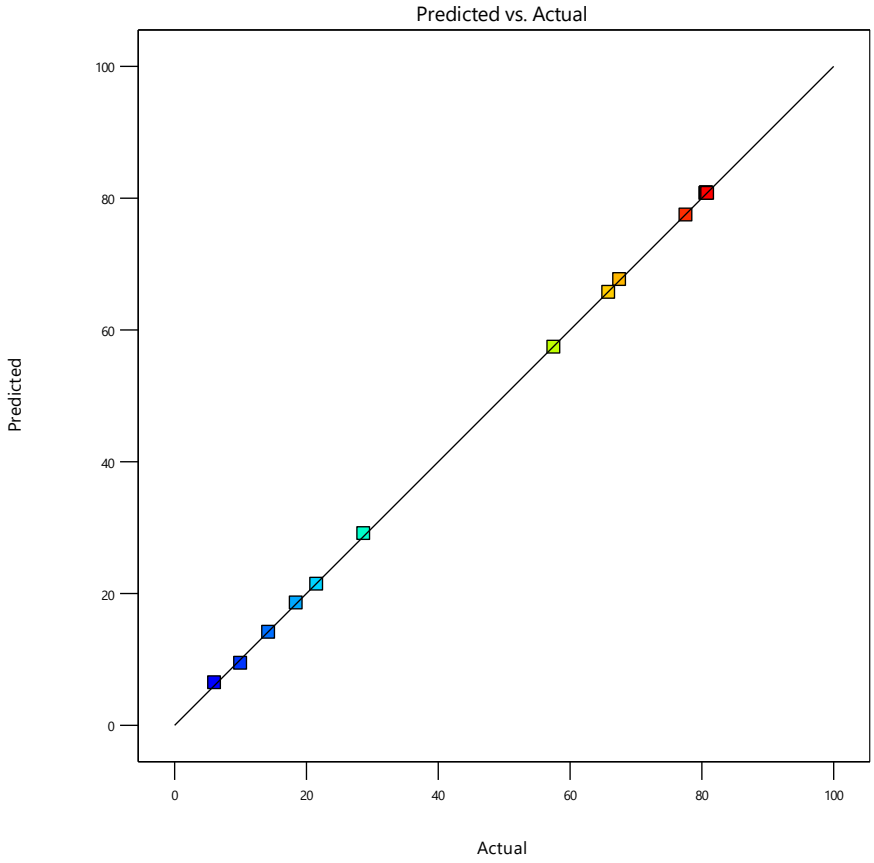

Figure 12. Predicted vs. actual measurements for R%.

The 3D surface response graph was plotted against two parameters to illustrate the combined effects of parameters on simultaneous photocatalytic degradation of BPB by $TiO_2/g\text{-}C_3N_4$ as shown in Figure 13.

In Figure 13a,b, the degradation efficiency reveals that lower pH leads to more photodegradation efficiency with approximately 75–80% of BPB removal at pH 3 and C_{H2O2} (0.4–2.4 mmol L^{-1}). At pH > 3 we observe a decrease in degradation and a gradual increase from pH 9 up to pH 11 where we observed a degradation efficiency of approximately 70% at C_{H2O2} ranging between 1.9 to 2.4 mmol/L.

Figure 13c,d showed similar results as the previous plot with photodegradation efficiency of approximately 75–80% of BPB removal at pH 3 and with C_{NaCl} (5–15 mgL^{-1}). At pH 11 there is a degradation efficiency of approximately 60% at C_{NaCl} (5–15 mgL^{-1}).

3.8. Reactive Oxygen Species Contribution

To determine the contribution of Reactive Oxygen Species (ROS) in the degradation of BPB by $TiO_2/g\text{-}C_3N_4$ under UV light illumination, different ROS trappers were used at sufficient concentrations to suppress the corresponding ROS. Isopropanol, methanol and potassium dichromate were used as specific trappers of hydroxyl radicals ($HO^{\bullet}$), holes (h^+) and superoxide ions ($O_2^{\bullet-}$) respectively in bulk solutions [24,84].

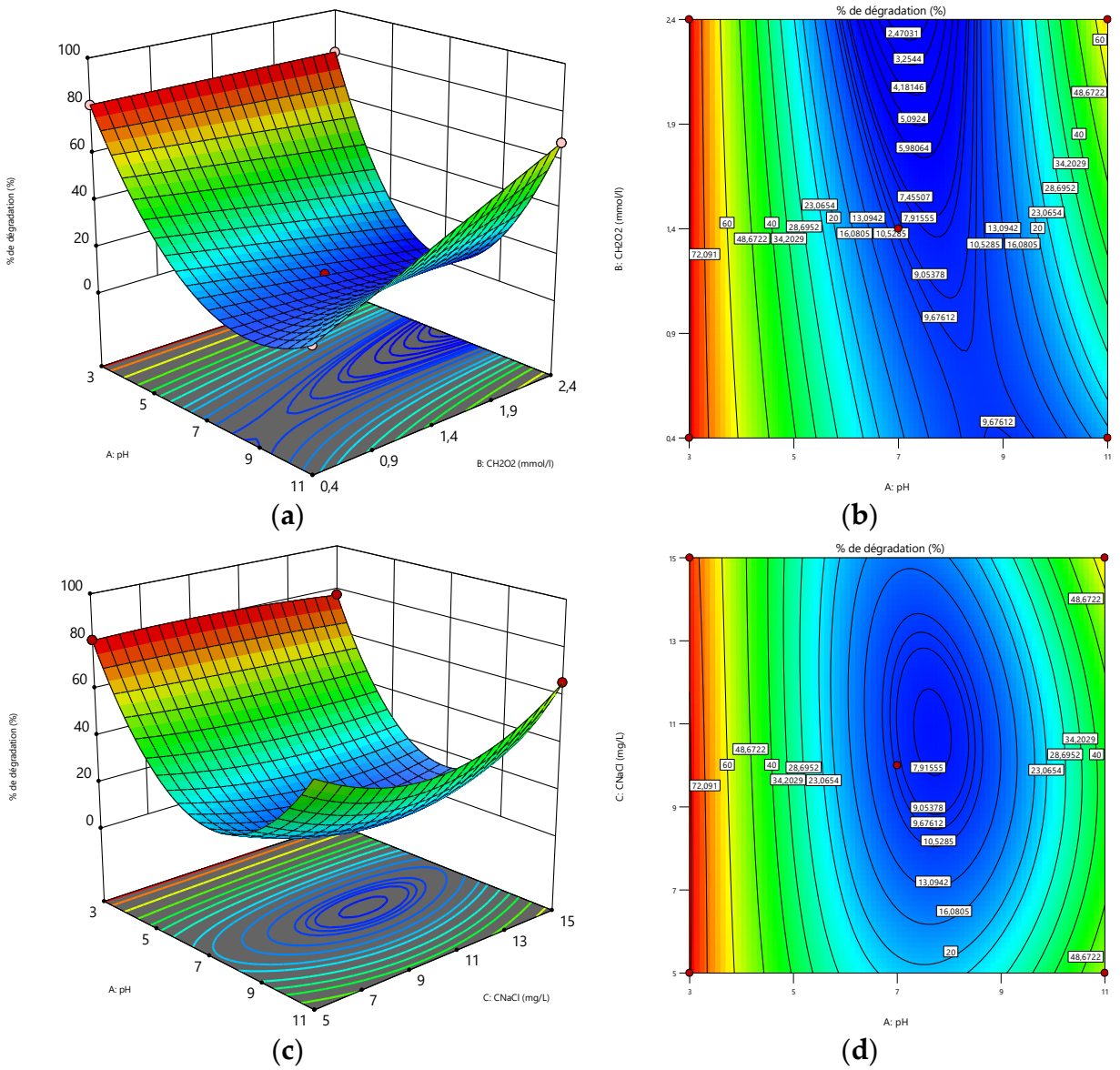

Figure 13. Response surface and contour plots for the mutual effects of pH, C_{NaCl}, and $C_{H_2O_2}$ on photocatalytic degradation BPB by TiO_2/g-C_3N_4.

The experiments were carried out by addition of 43.5 mM isopropanol (IsoPro), 50 mM methanol (MeOH), and 1.1 mM potassium dichromate ($K_2Cr_2O_7$) into a 500 mL BPB (10 ppm) to examine their impact on photocatalytic degradation of BPB with 100 mg/L of catalyst.

From Figure 14, the presence of these trappers in the TiO_2/g-C_3N_4 suspensions affected the BPB degradation, which suggested that all of the h^+, $HO^{\bullet -}$and $O_2^{\bullet -}$ contributed to the BPB degradation. Using IsoPro, MeOH and $K_2Cr_2O_7$ we obtained a degradation percentage of 71.87, 78.22 and 27.89%, respectively. From this result, Figure 14 confirmed that $O_2^{\bullet -}$ was the primary ROS involved in the photocatalytic degradation of BPB with 68.89% contribution followed by $HO^{\bullet}$ and h^+ with 22.40% and 15.55% contribution, respectively.

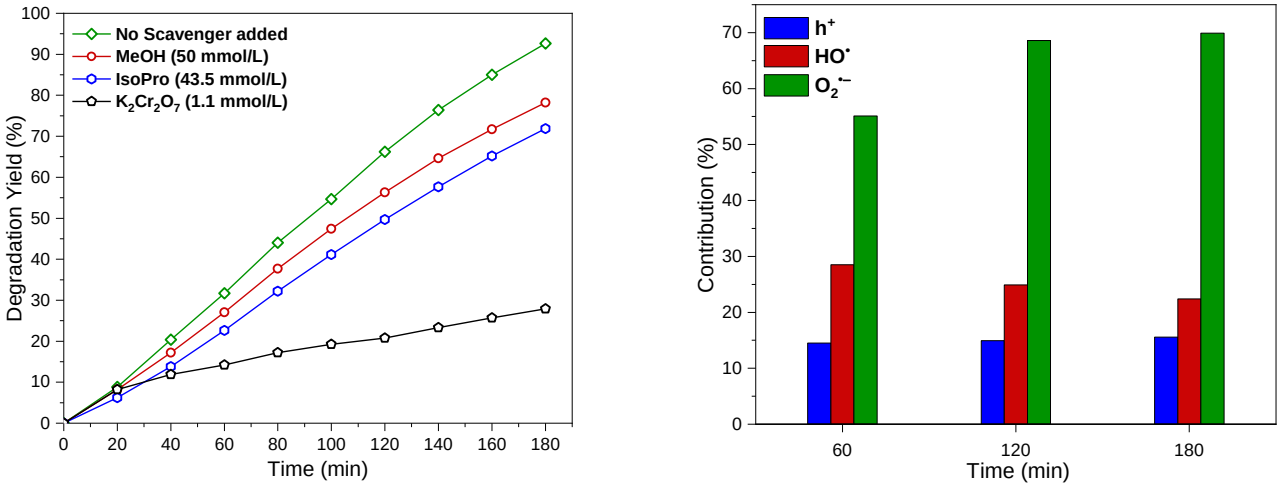

(**a**) (**b**)

Figure 14. (**a**) Effect of additives in the degradation of 10 ppm of BPB and (**b**) Contribution of various active species in the photodegradation (500 mL of BPB solution, natural pH, under UV irradiation).

The amount of radicals in the system involved in the dye degradation can differ significantly due to electron-hole recombination and recombination reactions of radical species [24].

Considering the scavenging tests, the photodegradation of BPB with the $TiO_2/g\text{-}C_3N_4$ catalyst could be described by following steps: $TiO_2/g\text{-}C_3N_4$ was excited by UV-light to generate electron-hole pairs with photogenerated electrons flowing from $g\text{-}C_3N_4$ to the surface of TiO_2. Part of the electrons produced by $g\text{-}C_3N_4$ are captured by the oxygen adsorbed on the surface, generating superoxide radicals ($O_2^{\bullet -}$) with strong oxidizing properties, then decomposing the pollutant in the wastewater, as shown in reactions below [85]:

$$TiO_2/g\text{-}C_3N_4 + h\nu \rightarrow e^- + h^+ \quad (15)$$

$$O_2 + e^- \rightarrow O_2^{\bullet -} \quad (16)$$

$$H_2O + h^+ \rightarrow OH^- + H^+ \quad (17)$$

$$h^+ + OH^- \rightarrow HO^{\bullet} \quad (18)$$

$$HO^{\bullet} + O_2^{\bullet -} + \text{pollution} \rightarrow \text{degradation products} \quad (19)$$

Researches on photocatalytic degradation of organic pollutants generally align with the fact that h^+ and $O_2^{\bullet -}$ are the main radical species using $g\text{-}C_3N_4$-based catalyst [78] which is slightly different from the results obtained.This implies that the presence of $g\text{-}C_3N_4$ with TiO_2 and UV irradiation can affect the physico-chemical properties of the photocatalyst and influence main radical species in the photocatalytic organic treatment process.

4. Conclusions

In this work, $TiO_2/g\text{-}C_3N_4$ was synthesized by wet- impregnation and applied in the photodegradation of EBT and BPB dye solutions. The heterojunction phenomenon in $TiO_2/g\text{-}C_3N_4$ facilitates the photoexcited charges transfer and simultaneously reduces photogenerated electron-hole recombination, which in turn markedly improves its photocatalytic performance which is higher than that of $g\text{-}C_3N_4$ alone. The degradation efficiency indicated that a decrease in initial dye concentration and increase in catalyst dosage positively affects photodegradation. The study of the degradation kinetics showed that the degradation of BPB follows both the pseudo-first-order kinetic and Langmuir-Hinshelwood model with an average value of R^2 equal to 0.979 and 0.975 respectively. The addition of $Na_2S_2O_8$ to the suspension increased the degradation rate in 20 min from 8.8% to 80% yield, an amplitude of 9.1. The optimization of the photodegradation of BPB was investigated

using CCD and RSM methodologies where R% reached maximum values at pH 3 in the presence of NaCl and H_2O_2. Isopropanol, methanol and potassium dichromate were used as scavenger radicals and $O_2^{\bullet-}$ were identified to be the predominant radical species in the photodegradation using TiO_2/g-C_3N_4 catalyst. The present work provides the efficient photocatalysts as a promising material for environmental remediation purposes.

Supplementary Materials: The following supporting information can be downloaded at: https://www.mdpi.com/article/10.3390/w14203331/s1, Figure S1: UV lamp spectrum (24 W); Figure S2: Photoctalytic degradation of BPB with TiO2/g-C3N4 under uv light (C_0: 10 ppm, Catalyst dose: 200 mg/L,V solution: 500 mL, natural pH).

Author Contributions: Conceptualization, H.Z. and A.K.; methodology, H.Z.; software, H.Z.; validation, H.Z., A.K., S.D., P.B. and C.C.; formal analysis, H.Z.; investigation, F.H., H.Z., P.B. and C.C.; writing—original draft preparation, F.H. and H.Z.; writing—review and editing, H.Z. and J.M.D.D.; visualization, H.Z., P.B. and C.C.; supervision, H.Z., A.K., S.D., P.B. and N.G.B. All authors have read and agreed to the published version of the manuscript.

Funding: This research received no external funding.

Data Availability Statement: Not applicable.

Acknowledgments: The authors would like to thank Ivane LELIEVRE (UniLaSalle Rennes) for their technical help and Jessica Wilson for her proofreading. The authors would like to acknowledge The Erasmus+ International Credit Mobility for the Grant (Grant agreement numbrer: 2019-1-FR01-KA107-060920) between Unilasalle Polytechnic Institute and University of Maroua. The authors would also like to acknowledge the financial support of the INTERREG NorthWest Europe ThreeC with the project number NWE 1010, under the umbrella of the European Regional Development Fund (ERDF).

Conflicts of Interest: The authors declare no conflict of interest.

References

1. Preisner, M. Surface Water Pollution by Untreated Municipal Wastewater Discharge Due to a Sewer Failure. *Environ. Process.* **2020**, *7*, 767–780. [CrossRef]
2. Rafiq, A.; Ikram, M.; Ali, S.; Niaz, F.; Khan, M.; Khan, Q.; Maqbool, M. Photocatalytic Degradation of Dyes Using Semiconductor Photocatalysts to Clean Industrial Water Pollution. *J. Ind. Eng. Chem.* **2021**, *97*, 111–128. [CrossRef]
3. Grigioni, I.; Stamplecoskie, K.G.; Selli, E.; Kamat, P.V. Dynamics of Photogenerated Charge Carriers in WO3/BiVO4 Heterojunction Photoanodes. *J. Phys. Chem. C* **2015**, *119*, 20792–20800. [CrossRef]
4. Assadi, I.; Guesmi, A.; Baaloudj, O.; Zeghioud, H.; Elfalleh, W.; Benhammadi, N.; Khezami, L.; Assadi, A.A. Review on Inactivation of Airborne Viruses Using Non-Thermal Plasma Technologies: From MS2 to Coronavirus. *Environ. Sci. Pollut. Res.* **2022**, *29*, 4880–4892. [CrossRef]
5. Wang, Q.; Yang, Z. Industrial Water Pollution, Water Environment Treatment, and Health Risks in China. *Environ. Pollut.* **2016**, *218*, 358–365. [CrossRef]
6. Dula, T.; Duke, T.N. Removal Methods of Heavy Metals from Laboratory Wastewater. *J. Nat. Sci. Res.* **2019**, *9*, 36–42. [CrossRef]
7. Zeghioud, H.; Fryda, L.; Djelal, H.; Assadi, A.; Kane, A.; Unilasalle-ecole, M. A Comprehensive Review of Biochar in Removal of Organic Pollutants from Wastewater: Characterization, Toxicity, Activation / Functionalization and Influencing Treatment Factors. *J. Water Process Eng.* **2022**, *47*, 102801. [CrossRef]
8. Awad, A.M.; Shaikh, S.M.R.; Jalab, R.; Gulied, M.H.; Nasser, M.S.; Benamor, A.; Adham, S. Adsorption of Organic Pollutants by Natural and Modified Clays: A Comprehensive Review. *Sep. Purif. Technol.* **2019**, *228*, 115719. [CrossRef]
9. Hasanzadeh, M.; Simchi, A.; Shahriyari Far, H. Nanoporous Composites of Activated Carbon-Metal Organic Frameworks for Organic Dye Adsorption: Synthesis, Adsorption Mechanism and Kinetics Studies. *J. Ind. Eng. Chem.* **2020**, *81*, 405–414. [CrossRef]
10. Chandrashekar Kollarahithlu, S.; Balakrishnan, R.M.; Delgado, N.; Capparelli, A.; Navarro, A.; Marino, D. Adsorption of Pharmaceuticals Pollutants, Ibuprofen, Acetaminophen, and Streptomycin from the Aqueous Phase Using Amine Functionalized Superparamagnetic Silica Nanocomposite. *J. Clean. Prod.* **2019**, *236*, 126155. [CrossRef]
11. Delgado, N.; Capparelli, A.; Navarro, A.; Marino, D. Pharmaceutical Emerging Pollutants Removal from Water Using Powdered Activated Carbon: Study of Kinetics and Adsorption Equilibrium. *J. Environ. Manage.* **2019**, *236*, 301–308. [CrossRef]
12. Mehdizadeh, P.; Orooji, Y.; Amiri, O.; Salavati-Niasari, M.; Moayedi, H. Green Synthesis Using Cherry and Orange Juice and Characterization of TbFeO3 Ceramic Nanostructures and Their Application as Photocatalysts under UV Light for Removal of Organic Dyes in Water. *J. Clean. Prod.* **2020**, *252*, 119765. [CrossRef]

13. Zeghioud, H.; Khellaf, N.; Djelal, H.; Amrane, A.; Bouhelassa, M. Photocatalytic Reactors Dedicated to the Degradation of Hazardous Organic Pollutants: Kinetics, Mechanistic Aspects, and Design—A Review. *Chem. Eng. Commun.* **2016**, *203*, 1415–1431. [CrossRef]
14. Wang, C.; Sun, R.; Huang, R.; Cao, Y. A Novel Strategy for Enhancing Heterogeneous Fenton Degradation of Dye Wastewater Using Natural Pyrite: Kinetics and Mechanism. *Chemosphere* **2021**, *272*, 129883. [CrossRef]
15. El Hassani, K.; Kalnina, D.; Turks, M.; Beakou, B.H.; Anouar, A. Enhanced Degradation of an Azo Dye by Catalytic Ozonation over Ni-Containing Layered Double Hydroxide Nanocatalyst. *Sep. Purif. Technol.* **2019**, *210*, 764–774. [CrossRef]
16. Ameen, S.; Shaheer Akhtar, M.; Shik Shin, H. Speedy Photocatalytic Degradation of Bromophenol Dye over ZnO Nanoflowers. *Mater. Lett.* **2017**, *209*, 150–154. [CrossRef]
17. He, Y.; Lin, H.; Guo, Z.; Zhang, W.; Li, H.; Huang, W. Recent Developments and Advances in Boron-Doped Diamond Electrodes for Electrochemical Oxidation of Organic Pollutants. *Sep. Purif. Technol.* **2019**, *212*, 802–821. [CrossRef]
18. Zeghioud, H.; Nguyen-Tri, P.; Khezami, L.; Amrane, A.; Assadi, A.A. Review on Discharge Plasma for Water Treatment: Mechanism, Reactor Geometries, Active Species and Combined Processes. *J. Water Process Eng.* **2020**, *38*, 101664. [CrossRef]
19. Dalhatou, S.; Pétrier, C.; Massaï, H.; Kouotou, P.M.; Laminsi, S.; Baup, S. Degradation of Endocrine Disrupting Chemical Nonylphenol in Aqueous Milieu Using High Frequency Ultrasound. *Int. J. Water Wastewater Treat.* **2016**, *2*. [CrossRef]
20. Wang, J.; Zhuan, R.; Chu, L. The Occurrence, Distribution and Degradation of Antibiotics by Ionizing Radiation: An Overview. *Sci. Total Environ.* **2019**, *646*, 1385–1397. [CrossRef]
21. Rueda-Marquez, J.J.; Levchuk, I.; Fernández Ibañez, P.; Sillanpää, M. A Critical Review on Application of Photocatalysis for Toxicity Reduction of Real Wastewaters. *J. Clean. Prod.* **2020**, *258*. [CrossRef]
22. Fang, M.; Tan, X.; Liu, Z.; Hu, B.; Wang, X. Recent Progress on Metal-Enhanced Photocatalysis: A Review on the Mechanism. *Research* **2021**, *2021*, 9794329. [CrossRef]
23. Liang, Q.; Liu, X.; Zeng, G.; Liu, Z.; Tang, L.; Shao, B.; Zeng, Z.; Zhang, W.; Liu, Y.; Cheng, M.; et al. Surfactant-Assisted Synthesis of Photocatalysts: Mechanism, Synthesis, Recent Advances and Environmental Application. *Chem. Eng. J.* **2019**, *372*, 429–451. [CrossRef]
24. Zeghioud, H.; Assadi, A.A.; Khellaf, N.; Djelal, H.; Amrane, A.; Rtimi, S. Reactive Species Monitoring and Their Contribution for Removal of Textile Effluent with Photocatalysis under UV and Visible Lights: Dynamics and Mechanism. *J. Photochem. Photobiol. A Chem.* **2018**, *365*, 94–102. [CrossRef]
25. Neppolian, B.; Kanel, S.R.; Choi, H.C.; Shankar, M.V.; Arabindoo, B.; Murugesan, V. Photocatalytic Degradation of Reactive Yellow 17 Dye in Aqueous Solution in the Presence of TiO_2 with Cement Binder. *Int. J. Photoenergy* **2003**, *5*, 45–49. [CrossRef]
26. Li, L.; Yuan, X.; Zhou, Z.; Tang, R.; Deng, Y.; Huang, Y.; Xiong, S.; Su, L.; Zhao, J.; Gong, D. Research Progress of Photocatalytic Activated Persulfate Removal of Environmental Organic Pollutants by Metal and Nonmetal Based Photocatalysts. *J. Clean. Prod.* **2022**, *372*, 133420. [CrossRef]
27. Sun, B.; Li, H.; Wei, Q.; Xue, S.; Zhou, A.; Yue, X. Enhanced Quinoline Degradation by Persulfate-Assisted Photocatalytic Process with WO3-CuFe2O4 Z-Scheme System: Properties and Mechanism. *Sep. Purif. Technol.* **2022**, *301*, 122039. [CrossRef]
28. Wen, J.; Xie, J.; Chen, X.; Li, X. A Review on G-C_3N_4 -Based Photocatalysts. *Appl. Surf. Sci.* **2017**, *391*, 72–123. [CrossRef]
29. Li, Y.; Zhou, M.; Cheng, B.; Shao, Y. Recent Advances in G-C_3N_4-Based Heterojunction Photocatalysts. *J. Mater. Sci. Technol.* **2020**, *56*, 1–17. [CrossRef]
30. Chen, D.; Cheng, Y.; Zhou, N.; Chen, P.; Wang, Y.; Li, K.; Huo, S.; Cheng, P.; Peng, P.; Zhang, R.; et al. Photocatalytic Degradation of Organic Pollutants Using TiO_2-Based Photocatalysts: A Review. *J. Clean. Prod.* **2020**, *268*, 121725. [CrossRef]
31. Xing, Z.; Zhang, J.; Cui, J.; Yin, J.; Zhao, T.; Kuang, J.; Xiu, Z.; Wan, N.; Zhou, W. Recent Advances in Floating TiO_2-Based Photocatalysts for Environmental Application. *Appl. Catal. B Environ.* **2018**, *225*, 452–467. [CrossRef]
32. Paumo, H.K.; Dalhatou, S.; Katata-Seru, L.M.; Kamdem, B.P.; Tijani, J.O.; Vishwanathan, V.; Kane, A.; Bahadur, I. TiO_2 Assisted Photocatalysts for Degradation of Emerging Organic Pollutants in Water and Wastewater. *J. Mol. Liq.* **2021**, *331*, 115458. [CrossRef]
33. Ge, M.; Hu, Z.; Wei, J.; He, Q.; He, Z. Recent Advances in Persulfate-Assisted TiO_2-Based Photocatalysis for Wastewater Treatment: Performances, Mechanism and Perspectives. *J. Alloys Compd.* **2021**, *888*, 161625. [CrossRef]
34. Nemiwal, M.; Zhang, T.C.; Kumar, D. Recent Progress in G-C_3N_4, TiO_2 and ZnO Based Photocatalysts for Dye Degradation: Strategies to Improve Photocatalytic Activity. *Sci. Total Environ.* **2021**, *767*, 144896. [CrossRef] [PubMed]
35. Li, Y.; Li, X.; Zhang, H.; Fan, J.; Xiang, Q. Design and Application of Active Sites in G-C_3N_4-Based Photocatalysts. *J. Mater. Sci. Technol.* **2020**, *56*, 69–88. [CrossRef]
36. Alcudia-Ramos, M.A.; Fuentez-Torres, M.O.; Ortiz-Chi, F.; Espinosa-González, C.G.; Hernández-Como, N.; García-Zaleta, D.S.; Kesarla, M.K.; Torres-Torres, J.G.; Collins-Martínez, V.; Godavarthi, S. Fabrication of G-C_3N_4/TiO_2 Heterojunction Composite for Enhanced Photocatalytic Hydrogen Production. *Ceram. Int.* **2020**, *46*, 38–45. [CrossRef]
37. Zhong, J.; Huang, J.; Liu, Y.; Li, D.; Tan, C.; Chen, P.; Liu, H.; Zheng, X.; Wen, C.; Lv, W.; et al. Construction of Double-Functionalized g-C_3N_4 Heterojunction Structure via Optimized Charge Transfer for the Synergistically Enhanced Photocatalytic Degradation of Sulfonamides and H2O2 Production. *J. Hazard. Mater.* **2022**, *422*, 126868. [CrossRef]
38. Liu, C.; Dong, S.S.; Chen, Y. Enhancement of Visible-Light-Driven Photocatalytic Activity of Carbon Plane/g-C_3N_4/TiO_2 Nanocomposite by Improving Heterojunction Contact. *Chem. Eng. J.* **2019**, *371*, 706–718. [CrossRef]
39. Wang, J.; Wang, G.; Cheng, B.; Yu, J.; Fan, J. Sulfur-Doped g-C_3N_4/TiO_2 S-Scheme Heterojunction Photocatalyst for Congo Red Photodegradation. *Chinese J. Catal.* **2020**, *42*, 56–68. [CrossRef]

40. Kansal, S.K.; Sood, S.; Umar, A.; Mehta, S.K. Photocatalytic Degradation of Eriochrome Black T Dye Using Well-Crystalline Anatase TiO_2Nanoparticles. *J. Alloys Compd.* **2013**, *581*, 392–397. [CrossRef]
41. Kazeminezhad, I.; Sadollahkhani, A. Photocatalytic Degradation of Eriochrome Black-T Dye Using ZnO Nanoparticles. *Mater. Lett.* **2014**, *120*, 267–270. [CrossRef]
42. Abdel-Khalek, A.A.; Mahmoud, S.A.; Zaki, A.H. Visible Light Assisted Photocatalytic Degradation of Crystal Violet, Bromophenol Blue and Eosin Y Dyes Using AgBr-ZnO Nanocomposite. *Environ. Nanotechnol. Monit. Manag.* **2018**, *9*, 164–173. [CrossRef]
43. Xing, Z.; Chen, Z.; Zong, X.; Wang, L. A New Type of Carbon Nitride-Based Polymer Composite for Enhanced Photocatalytic Hydrogen Production. *Chem. Commun.* **2014**, *50*, 6762–6764. [CrossRef] [PubMed]
44. Kane, A.; Chafiq, L.; Dalhatou, S.; Bonnet, P.; Nasr, M.; Gaillard, N.; Dikdim, J.M.D.; Monier, G.; Assadie, A.A.; Zeghioud, H. G-C_3N_4/TiO_2 S-Scheme Heterojunction Photocatalyst with Enhanced Photocatalytic Carbamazepine Degradation and Mineralization. *J. Photochem. Photobiol. A Chem.* **2022**, *430*, 113971. [CrossRef]
45. Askari, M.B.; Tavakoli Banizi, Z.; Seifi, M.; Bagheri Dehaghi, S.; Veisi, P. Synthesis of TiO_2 Nanoparticles and Decorated Multi-Wall Carbon Nanotube (MWCNT) with Anatase TiO_2 Nanoparticles and Study of Optical Properties and Structural Characterization of TiO_2/MWCNT Nanocomposite. *Optik Stuttg.* **2017**, *149*, 447–454. [CrossRef]
46. Pan, C.; Xu, J.; Wang, Y.; Li, D.; Zhu, Y. Dramatic Activity of C 3N 4/BiPO 4 Photocatalyst with Core/Shell Structure Formed by Self-Assembly. *Adv. Funct. Mater.* **2012**, *22*, 1518–1524. [CrossRef]
47. Senthil, R.A.; Theerthagiri, J.; Selvi, A.; Madhavan, J. Synthesis and Characterization of Low-Cost g-C_3N_4/TiO_2 Composite with Enhanced Photocatalytic Performance under Visible-Light Irradiation. *Opt. Mater.* **2017**, *64*, 533–539. [CrossRef]
48. Nair, R.V.; Jijith, M.; Gummaluri, V.S.; Vijayan, C. A Novel and Efficient Surfactant-Free Synthesis of Rutile TiO_2 Microflowers with Enhanced Photocatalytic Activity. *Opt. Mater.* **2016**, *55*, 38–43. [CrossRef]
49. Boonprakob, N.; Wetchakun, N.; Phanichphant, S.; Waxler, D.; Sherrell, P.; Nattestad, A.; Chen, J.; Inceesungvorn, B. Enhanced Visible-Light Photocatalytic Activity of g-C_3N_4/TiO_2 Films. *J. Colloid Interface Sci.* **2014**, *417*, 402–409. [CrossRef]
50. Sathishkumar, K.; Li, Y.; Alsalhi, M.S.; Muthukumar, B.; Gaurav, G.K.; Devanesan, S.; Rajasekar, A.; Manikandan, R. Enhanced Biological Nitrate Removal by GC_3N_4/TiO_2 Composite and Role of Extracellular Polymeric Substances. *Environ. Res.* **2022**, *207*, 112158. [CrossRef]
51. Challagulla, S.; Tarafder, K.; Ganesan, R.; Roy, S. Structure Sensitive Photocatalytic Reduction of Nitroarenes over TiO_2. *Sci. Rep.* **2017**, *7*, 8783. [CrossRef] [PubMed]
52. Su, W.; Zhang, J.; Feng, Z.; Chen, T.; Ying, P.; Li, C. Surface Phases of TiO_2 Nanoparticles Studied by UV Raman Spectroscopy and FT-IR Spectroscopy. *J. Phys. Chem. C* **2008**, *112*, 7710–7716. [CrossRef]
53. Yan, S.C.; Lv, S.B.; Li, Z.S.; Zou, Z.G. Organic-Inorganic Composite Photocatalyst of g-C_3N_4 and TaON with Improved Visible Light Photocatalytic Activities. *Dalt. Trans.* **2010**, *39*, 1488–1491. [CrossRef] [PubMed]
54. Wang, Y.; Shi, R.; Lin, J.; Zhu, Y. Enhancement of Photocurrent and Photocatalytic Activity of ZnO Hybridized with Graphite-like C_3N_4. *Energy Environ. Sci.* **2011**, *4*, 2922–2929. [CrossRef]
55. Hu, S.; Yuan, J.; Tang, S.; Luo, D.; Shen, Q.; Qin, Y.; Zhou, J.; Tang, Q.; Chen, S.; Luo, X.; et al. Perovskite-Type $SrFeO_3$/g-C_3N_4 S-Scheme Photocatalyst for Enhanced Degradation of Acid Red B. *Opt. Mater.* **2022**, *132*. [CrossRef]
56. Yang, J.; Wu, X.; Li, X.; Liu, Y.; Gao, M.; Liu, X.; Kong, L.; Yang, S. Synthesis and Characterization of Nitrogen-Rich Carbon Nitride Nanobelts by Pyrolysis of Melamine. *Appl. Phys. A Mater. Sci. Process.* **2011**, *105*, 161–166. [CrossRef]
57. Chai, B.; Peng, T.; Mao, J.; Li, K.; Zan, L. Graphitic Carbon Nitride (g-C 3N 4)-Pt-TiO 2 Nanocomposite as an Efficient Photocatalyst for Hydrogen Production under Visible Light Irradiation. *Phys. Chem. Chem. Phys.* **2012**, *14*, 16745–16752. [CrossRef]
58. Yan, H.; Yang, H. TiO_2-g-C_3N_4 Composite Materials for Photocatalytic H 2 Evolution under Visible Light Irradiation. *J. Alloys Compd.* **2011**, *509*, 26–29. [CrossRef]
59. Wang, S.; Li, D.; Sun, C.; Yang, S.; Guan, Y.; He, H. Synthesis and Characterization of G-C_3N_4/Ag_3VO_4 Composites with Significantly Enhanced Visible-Light Photocatalytic Activity for Triphenylmethane Dye Degradation. *Appl. Catal. B Environ.* **2014**, *144*, 885–892. [CrossRef]
60. Monga, D.; Basu, S. Enhanced Photocatalytic Degradation of Industrial Dye by G-C_3N_4 /TiO_2 Nanocomposite: Role of Shape of TiO2. *Adv. Powder Technol.* **2019**, *30*, 1089–1098. [CrossRef]
61. Sharma, M.; Vaidya, S.; Ganguli, A.K. Enhanced Photocatalytic Activity of G-C_3N_4-TiO_2 Nanocomposites for Degradation of Rhodamine B Dye. *J. Photochem. Photobiol. A Chem.* **2017**, *335*, 287–293. [CrossRef]
62. Shafawi, A.N.; Mahmud, R.A.; Ahmed Ali, K.; Putri, L.K.; Md Rosli, N.I.; Mohamed, A.R. Bi_2O_3 Particles Decorated on Porous G-C_3N_4 Sheets: Enhanced Photocatalytic Activity through a Direct Z-Scheme Mechanism for Degradation of Reactive Black 5 under UV–Vis Light. *J. Photochem. Photobiol. A Chem.* **2020**, *389*. [CrossRef]
63. Guo, Z.; Ni, S.; Wu, H.; Wen, J.; Li, X.; Tang, T.; Li, M.; Liu, M. Designing Nitrogen and Phosphorus Co-Doped Graphene Quantum Dots/g-C_3N_4 Heterojunction Composites to Enhance Visible and Ultraviolet Photocatalytic Activity. *Appl. Surf. Sci.* **2021**, *548*, 149211. [CrossRef]
64. Song, G.; Chu, Z.; Jin, W.; Sun, H. Enhanced Performance of G-C_3N_4/TiO_2 Photocatalysts for Degradation of Organic Pollutants under Visible Light. *Chinese J. Chem. Eng.* **2015**, *23*, 1326–1334. [CrossRef]

65. Tameu Djoko, S.Y.; Bashiri, H.; Njoyim, E.T.; Arabameri, M.; Djepang, S.; Tamo, A.K.; Laminsi, S.; Tasbihi, M.; Schwarze, M.; Schomäcker, R. Urea and Green Tea like Precursors for the Preparation of G-C_3N_4 Based Carbon Nanomaterials (CNMs) Composites as Photocatalysts for Photodegradation of Pollutants under UV Light Irradiation. *J. Photochem. Photobiol. A Chem.* **2020**, *398*, 112596. [CrossRef]
66. Zhu, X.; Wang, Y.; Guo, Y.; Wan, J.; Yan, Y.; Zhou, Y.; Sun, C. Environmental-Friendly Synthesis of Heterojunction Photocatalysts g-C_3N_4/$BiPO_4$ with Enhanced Photocatalytic Performance. *Appl. Surf. Sci.* **2021**, *544*, 148872. [CrossRef]
67. Moradi, M.; Kakavandi, B.; Bahadoran, A.; Giannakis, S.; Dehghanifard, E. Intensification of Persulfate-Mediated Elimination of Bisphenol A by a Spinel Cobalt Ferrite-Anchored g-C_3N_4 S-Scheme Photocatalyst: Catalytic Synergies and Mechanistic Interpretation. *Sep. Purif. Technol.* **2022**, *285*, 120313. [CrossRef]
68. Bechambi, O.; Sayadi, S.; Najjar, W. Photocatalytic Degradation of Bisphenol A in the Presence of C-Doped ZnO: Effect of Operational Parameters and Photodegradation Mechanism. *J. Ind. Eng. Chem.* **2015**, *32*, 201–210. [CrossRef]
69. Kiwaan, H.A.; Atwee, T.M.; Azab, E.A.; El-Bindary, A.A. Photocatalytic Degradation of Organic Dyes in the Presence of Nanostructured Titanium Dioxide. *J. Mol. Struct.* **2020**, *1200*, 127115. [CrossRef]
70. Isai, K.A.; Shrivastava, V.S. Photocatalytic Degradation of Methylene Blue Using ZnO and 2%Fe–ZnO Semiconductor Nanomaterials Synthesized by Sol–Gel Method: A Comparative Study. *SN Appl. Sci.* **2019**, *1*, 1247. [CrossRef]
71. Ebrahimi, R.; Maleki, A.; Zandsalimi, Y.; Ghanbari, R.; Shahmoradi, B.; Rezaee, R.; Safari, M.; Joo, S.W.; Daraei, H.; Harikaranahalli Puttaiah, S.; et al. Photocatalytic Degradation of Organic Dyes Using WO_3 -Doped ZnO Nanoparticles Fixed on a Glass Surface in Aqueous Solution. *J. Ind. Eng. Chem.* **2019**, *73*, 297–305. [CrossRef]
72. Alkaykh, S.; Mbarek, A.; Ali-Shattle, E.E. Photocatalytic Degradation of Methylene Blue Dye in Aqueous Solution by MnTiO3 Nanoparticles under Sunlight Irradiation. *Heliyon* **2020**, *6*, e03663. [CrossRef]
73. Vishnuganth, M.A.; Remya, N.; Kumar, M.; Selvaraju, N. Photocatalytic Degradation of Carbofuran by TiO_2-Coated Activated Carbon: Model for Kinetic, Electrical Energy per Order and Economic Analysis. *J. Environ. Manage.* **2016**, *181*, 201–207. [CrossRef]
74. Zamri, M.S.F.A.; Sapawe, N. Kinetic Study on Photocatalytic Degradation of Phenol Using Green Electrosynthesized TiO_2 Nanoparticles. *Mater. Today Proc.* **2019**, *19*, 1261–1266. [CrossRef]
75. Vasanth Kumar, K.; Porkodi, K.; Selvaganapathi, A. Constrain in Solving Langmuir-Hinshelwood Kinetic Expression for the Photocatalytic Degradation of Auramine O Aqueous Solutions by ZnO Catalyst. *Dye. Pigment.* **2007**, *75*, 246–249. [CrossRef]
76. Hamad, H.A.; Sadik, W.A.; Abd El-latif, M.M.; Kashyout, A.B.; Feteha, M.Y. Photocatalytic Parameters and Kinetic Study for Degradation of Dichlorophenol-Indophenol (DCPIP) Dye Using Highly Active Mesoporous TiO_2 Nanoparticles. *J. Environ. Sci.* **2016**, *43*, 26–39. [CrossRef]
77. Zeghioud, H.; Assadi, A.A.; Khellaf, N.; Djelal, H.; Amrane, A.; Rtimi, S. Photocatalytic Performance of Cu_xO/TiO_2 Deposited by HiPIMS on Polyester under Visible Light LEDs: Oxidants, Ions Effect, and Reactive Oxygen Species Investigation. *Materials* **2019**, *12*, 412. [CrossRef]
78. Hasija, V.; Nguyen, V.H.; Kumar, A.; Raizada, P.; Krishnan, V.; Khan, A.A.P.; Singh, P.; Lichtfouse, E.; Wang, C.; Thi Huong, P. Advanced Activation of Persulfate by Polymeric G-C_3N_4 Based Photocatalysts for Environmental Remediation: A Review. *J. Hazard. Mater.* **2021**, *413*, 125324. [CrossRef] [PubMed]
79. Ahmadi, M.; Ghanbari, F.; Moradi, M. Photocatalysis Assisted by Peroxymonosulfate and Persulfate for Benzotriazole Degradation: Effect of Ph on Sulfate and Hydroxyl Radicals. *Water Sci. Technol.* **2015**, *72*, 2095–2102. [CrossRef] [PubMed]
80. Chen, G.; Yu, Y.; Liang, L.; Duan, X.; Li, R.; Lu, X.; Yan, B.; Li, N.; Wang, S. Remediation of Antibiotic Wastewater by Coupled Photocatalytic and Persulfate Oxidation System: A Critical Review. *J. Hazard. Mater.* **2021**, *408*, 124461. [CrossRef]
81. Zubair, M.; Aziz, H.A.; Ihsanullah, I.; Ahmad, M.A.; Al-Harthi, M.A. Biochar Supported CuFe Layered Double Hydroxide Composite as a Sustainable Adsorbent for Efficient Removal of Anionic Azo Dye from Water. *Environ. Technol. Innov.* **2021**, *23*, 101614. [CrossRef]
82. Salehi, E.; Askari, M.; Velashjerdi, M.; Arab, B. Phosphoric Acid-Treated Spent Tea Residue Biochar for Wastewater Decoloring: Batch Adsorption Study and Process Intensification Using Multivariate Data-Based Optimization. *Chem. Eng. Process.-Process Intensif.* **2020**, *158*, 108170. [CrossRef]
83. AlAmeri, K.; Giwa, A.; Yousef, L.; Alraeesi, A.; Taher, H. Sorption and Removal of Crude Oil Spills from Seawater Using Peat-Derived Biochar: An Optimization Study. *J. Environ. Manage.* **2019**, *250*, 109465. [CrossRef] [PubMed]
84. Ismail, L.; Rifai, A.; Ferronato, C.; Fine, L.; Jaber, F.; Chovelon, J.M. Towards a Better Understanding of the Reactive Species Involved in the Photocatalytic Degradation of Sulfaclozine. *Appl. Catal. B Environ.* **2016**, *185*, 88–99. [CrossRef]
85. Zhang, M.; Han, N.; Fei, Y.; Liu, J.; Xing, L.; Núñez-Delgado, A.; Jiang, M.; Liu, S. TiO_2/g-C_3N_4 Photocatalyst for the Purification of Potassium Butyl Xanthate in Mineral Processing Wastewater. *J. Environ. Manag.* **2021**, *297*, 113311. [CrossRef] [PubMed]